Bending and Position Hysteresis of Magnetic Microfibers in Nonuniform Magnetic Fields

Richard E. Groff, Ph.D., Meng Li, Harshwardhan Karve, Alexander Tokarev, Kostantin G. Kornev

Clemson University, Clemson, SC UNITED STATES

Correspondence to:
Richard E. Groff email: regroff@clemson.edu

ABSTRACT

Magnetic microfibers are fibers that behave as a flexible paramagnetic body, for example, polymer fibers filled with superparamagnetic particles. A cantilevered magnetic microfiber will bend in response to an applied magnetic field. In a nonuniform field, generated for example by a single electromagnet or by a magnetic dipole, a magnetic microfiber displays position hysteresis as the field strength increases and decreases. This paper presents a model for determining stable shapes of a cantilevered magnetic microfiber in a nonuniform magnetic field. The model determines stable shapes by finding local minima of the potential energy using a Rayleigh-Ritz method. The model predicts the position hysteresis behavior observed in magnetic microfibers. Experimental data ware collected using two electromagnets with different geometries. The model simulation and experimental data compare well both qualitatively and quantitatively. The model will be useful for designing actuators based on magnetic microfibers and for characterizing the magnetic properties of fabricated fibers. A rigid bar model is also introduced, which captures the qualitative behavior of the fiber and illustrates the source of the position hysteresis behavior.

INTRODUCTION

A slender, flexible, unconstrained paramagnetic body in a uniform magnetic field will be acted on by torques that will cause the body to align itself with the direction of the field. In a nonuniform magnetic field, the body will additionally be acted on by forces that cause the body to move toward regions where the field has higher magnitude. If such a paramagnetic body is cantilevered, it will bend in the direction of an applied magnetic field, produced for example by an electromagnet.

Magnetic microfibers are fibers that act as a flexible paramagnetic body. The fibers used in the experimental section of this paper are hollow fibers filled with superparamagnetic nanoparticles. The model presented in the paper applies more broadly to magnetic microfibers, which includes the variety of paramagnetic composite fibers, such as found in [1-4].

More generally, magnetic microfibers are being investigated for potential use as electromagnetically actuated, fiber-based manipulators for microfluidic applications. The manipulators consist of a cantilevered fiber, typically 1-5cm in length, positioned between electromagnets with axes orthogonal to the fiber. Magnetic microfibers offer an additional tool for mesoscale fluid manipulation, for example picking and placing drops of liquid in lab-on-a-chip applications. The present work is specifically motivated by the use of magnetic microfibers as the basis for an artificial butterfly proboscis [4].

For a typical configuration of electromagnet and fiber, there will be a single stable shape when the magnitude of the magnetic field is small or large. When the magnitude of the magnetic field is in an intermediate range, there are two stable shapes that the fiber can take. This leads to hysteresis in the position of the fiber as the field is changed from low to high and back again. This hysteresis was first observed experimentally. One important objective of this paper is to provide a model that accurately captures this behavior.

Recent interest in magnetic microfibers has been driven by new methods of fabricating paramagnetic composite fibers and new applications for the fibers [1-9]. Much of the recent magnetic microfiber modeling effort builds directly on the analysis of paramagnetic beads in magnetostatic fields [10], which has a long history in the literature, motivated initially by the use of ligand-decorated paramagnetic beads for separating compounds out of solution. Paramagnetic particles in colloids form into chains in the presence of external fields, the dynamics of which are analyzed in [5,6]. Micrometer-sized

superparamagnetic beads have been linked together to form a permanent chain using a polymer linker, such as DNA or polyethylene glycol, between individual particles, creating very thin paramagnetic bead chains [1,2,7]. A chain of paramagnetic beads was attached to a red blood cell to create an artificial flagellum, driven by an externally applied magnetic field [7]. A number of variations on magnetic flagella and magnetic micropropulsion have appeared, including [8,9], though the latter uses a rigid helix rather than a flexible chain. Flexible paramagnetic chains have been analyzed using a number of methods, including dipole models [8] and energy methods relying on a demagnetizating factor approximation of the magnetic field [1,2,11-13]. In general, these papers assume that the applied magnetic field is uniform. Magnetic materials in a uniform field experience only torques, whereas in a nonuniform field they experience torques and forces.

Four decades ago, Moon et al. published several papers on magnetoelastic buckling of thin plates in uniform magnetostatic fields [14-16]. The plates were ferromagnetic, but were modeled as a linear magnetic material. This early work has been rarely cited in the recent efforts to model magnetic fibers; instead, the recent efforts build off of the literature on paramagnetic particles. Nevertheless, the energy methods and field approximations employed by Moon et al. bear many similarities to the techniques used in magnetic fiber models, including the model presented in this paper. In general, only uniform magnetic fields are considered [14-16]. The bending and vibration behavior of a ferromagnetic beam in a nonuniform field is considered in [17], but under the simplifying assumption that only the beam tip is affected by the external magnetic field.

This paper presents a continuum model of a cantilevered magnetic microfiber. The model predicts the stable shape or shapes of the fiber in an arbitrary *nonuniform* magnetostatic field. The model is derived based on energy methods. Specifically, local minima of the fiber potential energy are found using a Rayleigh-Ritz method. The paper presents a comparison of the simulated model with experimental data and discusses the position hysteresis that is predicted by the model as well as observed experimentally. Finally, a simplified model, the rigid bar model, is presented. The rigid bar model illustrates how the hysteresis behavior arises from the appearance and disappearance of local minima in the energy landscape.

MODELING MAGNETIC MICROFIBERS

The model presented here predicts the stable shape or shapes of a paramagnetic microfiber in the presence of a magnetostatic field. Similar to [1,3,12], the model uses energy techniques with a demagnetizing factor approximation of the magnetic field inside the fiber.

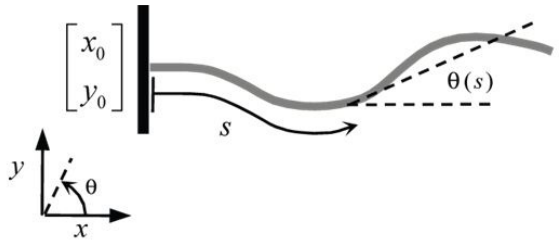

FIGURE 1. Coordinate system for the fiber configuration. The shape of the fiber is represented by $\theta(s)$.

The current work differs from previous efforts in that the external magnetic field is permitted to be nonuniform, requiring validation of the demagnetizing factor approximation as well as a different approach to the energy minimization.

A stable shape of the fiber corresponds to a local minimum of the fiber's potential energy. The potential energy of the fiber, consists of two components:

$$U = U_s + U_m \tag{1}$$

the strain potential energy U_s due to the work required to bend the fiber into a particular shape, and the magnetic potential energy U_m due to interaction between an externally generated magnetic field and the fiber's magnetic material. Both of these potentials depend on $\theta(s)$, the shape of the fiber, where $s \in [0, L]$ is the distance along the fiber as measured from the cantilevered end, and $\theta(s)$ is the angle of the fiber at distance s along the fiber, measured relative to the world frame. See *Figure 1*. This is the same parameterization of shape used in Euler elastica. The position of the fiber element that is distance s from the base is given by

$$\begin{bmatrix} x(s) \\ y(s) \end{bmatrix} = \begin{bmatrix} x_0 \\ y_0 \end{bmatrix} + \int_0^s \begin{bmatrix} \cos\theta(s) \\ \sin\theta(s) \end{bmatrix} ds \tag{2}$$

where $\begin{bmatrix} x_0 & y_0 \end{bmatrix}^{\mathrm{T}}$ is the location of the cantilevered base of the fiber. Representing fiber shape by $\theta(s)$ implicitly enforces the constraint that the fiber does not stretch along its axis. Moreover, the representation also assumes that the fiber moves within a plane. The latter assumption could be relaxed by using a more general representation borrowed from rod theory.

The strain energy for a linearly elastic rod is

$$U_s = \tfrac{1}{2}\int_0^L EI\left(\frac{d\theta}{ds}\right)^2 ds \tag{3}$$

where E is the elastic or Young's modulus, I is the cross-sectional moment of inertia, and L is the length of the fiber [18]. This expression assumes that the *strains* in the fiber, proportional to $d\theta/ds$, are small enough to produce linear stresses, but does *not* require that the angle or displacement of the fiber be small.

The magnetic potential is more complicated. In order to provide a unified presentation of the modeling assumptions used to approximate the magnetic potential energy, a detailed derivation is provided.

All materials will be assumed to be magnetically linear and isotropic. That is, the magnetic flux density B is related to the magnetic field strength H by a scalar parameter, i.e. $\mathrm{B} = \mu\mathrm{H}$, where μ is a material-dependent constant called the magnetic permeability. The permeability may be rewritten as $\mu = (1+\chi)\mu_0$, where $\mu_0 = 4\pi\times10^{-7}$ H/m is the permeability of free space and χ is a dimensionless material-dependent constant called the magnetic susceptibility. For a paramagnetic material, χ is positive but small, typically in the range of 10^{-5}-10^{-2} [19]. In comparison, the magnetic susceptibility for ferromagnetic materials is positive but several orders of magnitude higher than a paramagnetic material. Magnetic microfibers typically contain superparamagnetic nanoparticles. Superparamagnetic nanoparticles are composed of ferromagnetic material but, due to the extremely small particle size, cannot maintain a permanent magnetic field; hence, they behave as a paramagnetic material with magnetic susceptibility toward the upper end of the range for paramagnetic materials [20].

The total energy stored in a magnetic field is given by

$$T = \tfrac{1}{2}\int_V \mathrm{H}\bullet\mathrm{B}\,dV = \tfrac{1}{2}\int_V \mu|\mathrm{H}|^2\,dV \tag{4}$$

where the volume V is all space and the fields H and B are position dependent but static, i.e. H is produced by a set of constant current sources. The permeability μ is also position dependent, representing different objects at different locations.
Consider a new material, specifically the fiber in this case, introduced into the space, changing the permeability to be μ_f and susceptibility to be χ_f in volume V_f, without changing permeability anywhere else, while the currents that produced H continue to be held constant. The introduction of the magnetic material causes the resulting magnetic field H' and flux density B' to differ from the original magnetic field H and flux density B both inside and outside of volume V_f. Analogous to Eq. (4), the total energy stored in the new magnetic field is

$$T' = \tfrac{1}{2}\int_V \mathrm{H}'\bullet\mathrm{B}'\,dV \tag{5}$$

A theorem by Stratton [21] allows the change in total energy, $\Delta T = T' - T$, to be expressed more conveniently as,

$$\begin{aligned}\Delta T &= \tfrac{1}{2}\int_{V_f} (\mathrm{H}\bullet\mathrm{B}' - \mathrm{H}'\bullet\mathrm{B})\,dV \\ &= \tfrac{1}{2}\int_{V_f} (\mu_f - \mu)(\mathrm{H}'\bullet\mathrm{H})\,dV\end{aligned} \tag{6}$$

where integration is over just the volume of the fiber rather than all space. The integral depends on both H and H'. The field H' depends on the shape of the fiber, but fiber shape depends on energy, which in turn depends on the field H'. To solve this problem, H' will be approximated as a perturbation of H using demagnetizing factors, similar to the approximations used in [1,11,12].

If H is uniform and the magnetic object is a second order surface, such as an ellipsoid or infinitely long straight cylinder, then the field H' inside the body is also uniform and can be computed exactly using the demagnetizing factor associated with the shape of the body [20]. If the body is not a second order surface, an approximation of H' can still be computed for a wide variety of other body geometries. These are very good approximations, particularly for slender bodies [20,22].

In [1,11,12], the demagnetizing factor for an infinitely long, straight cylinder is used to predict H' inside a curved fiber placed in a uniform applied field H. In the present work, the demagnetizing factor approximation is further extended to predict H' inside a curved, paramagnetic fiber in a nonuniform field H. To apply the demagnetizing factor approximation in this case, H and H' are treated as locally uniform and constant across cross-sections of the fiber. Finite element simulations presented in the next section indicate that the demagnetizing factor approximations work quite well in uniform and nonuniform fields for the field strengths and fiber shapes of interest. In the following discussion, the demagnetizing factor approximations for uniform and nonuniform fields differ only in whether or not H is position dependent.

To compute the demagnetizating factor approximation, consider a long slender body lying in the x-y plane with shape described by $\theta(s)$. The initial field is $\mathrm{H} = H_x\vec{i} + H_y\vec{j}$ at the point $\left[x(s)\ \ y(s)\right]^{\mathrm{T}}$ on the axis of the fiber. The vector H may also be written in terms of components $H_{\|}$ and $H_{\perp}$, parallel and orthogonal to the fiber axis, respectively:

$$\begin{aligned} H_{\|}(\theta(s)) &= \ \ H_x\cos\theta(s) + H_y\sin\theta(s) \\ H_{\perp}(\theta(s)) &= -H_x\sin\theta(s) + H_y\cos\theta(s) \end{aligned} \tag{7}$$

Note also that in a nonuniform magnetic field, H_x and H_y depend on position $\left[x(s)\ \ y(s)\right]^{\mathrm{T}}$ and hence on the *function* $\theta(s)$ as seen in Eq. (2). The geometry-dependent demagnetizing factors predict that the resulting field in the corresponding cross-section of the fiber will be

$$\begin{aligned} H'_{\|} &= H_{\|} - N_{\|}M_{\|}, \\ H'_{\perp} &= H_{\perp} - N_{\perp}M_{\perp}. \end{aligned} \tag{8}$$

where $M_{\|}$ and $M_{\perp}$ are the magnetization of the material in the cross section, and $N_{\|}$ and $N_{\perp}$ are the demagnetizing factors. The fiber will be modeled as an infinitely long cylinder or needle, for which the demagnetizing factors are

$$N_{\|} = 0, \quad N_{\perp} = \tfrac{1}{2} \tag{9}$$

Moreover, magnetization for a linearly magnetic material is given by $M_{\|} = \chi_f H'_{\|}$ and $M_{\perp} = \chi_f H'_{\perp}$, where χ_f is the magnetic susceptibility of the fiber. Thus,

$$\begin{aligned} H'_{\|}(\theta(s)) &= \frac{H_{\|}(\theta(s))}{1+\chi_f N_{\|}} = H_{\|}(\theta(s)), \\ H'_{\perp}(\theta(s)) &= \frac{H_{\perp}(\theta(s))}{1+\chi_f N_{\perp}} = \frac{H_{\perp}(\theta(s))}{1+\frac{1}{2}\chi_f}. \end{aligned} \tag{10}$$

to determine the change in the total energy stored in the magnetic field for a fiber with cross sectional area A moving in air ($\mu = \mu_0$), substitute Eq. (10) into Eq. (6) and simplify appropriately, which yields

$$\Delta T = \tfrac{1}{2}A\chi_f\mu_0\int_0^L\left[H_{\|}^{\,2}(\theta(s)) + \frac{1}{1+\frac{1}{2}\chi_f}H_{\perp}^{\,2}(\theta(s))\right]ds. \tag{11}$$

The change in total energy stored in the field is the sum of two components: the first associated with the forces exerted on the source currents by the movement of the magnetic material and the second associated with the momentary increase in voltage necessary to keep the source currents constant [21]. The former component is the magnetic potential energy U_m, and it is half the magnitude and opposite in sign from the latter component. It follows that

$$U_m = -\Delta T \tag{12}$$

The total potential energy of the fiber is thus

$$\begin{aligned} U &= U_s + U_m \\ &= \int_0^L F(x, y, \theta, \dot{\theta}, s)\, ds \end{aligned} \tag{13}$$

where $\dot{\theta} = d\theta/ds$ and $F(x, y, \theta, \dot{\theta}, s)$ is given by

$$F(x, y, \theta, \dot{\theta}, s) = \frac{1}{2}\left[EI\left(\frac{d\theta}{ds}\right)^2 - A\chi_f\mu_0\left[H_{\|}^{\,2}(\theta(s)) + \frac{1}{1+\frac{1}{2}\chi_f}H_{\perp}^{\,2}(\theta(s))\right]\right] \tag{14}$$

The dependence of the integrand on x and y arises from the $H_{\|}$ and $H_{\perp}$ terms in the case of a nonuniform magnetic field. If the magnetic field is uniform, as in [1,12,13] then the position dependence falls away, i.e. $F(x, y, \theta, \dot{\theta}, s) = \bar{F}(\theta, \dot{\theta}, s)$. In this special case, the Euler-Lagrange necessary conditions from the calculus of variations provide a scalar ordinary differential equation boundary value problem whose solution is the minimum energy shape of the fiber. Specifically, for a uniform magnetic field, the Euler-Lagrange equation is

$$\begin{aligned} \ddot{\theta} &= -\frac{A\chi_f\mu_0 H_{\|}(\theta)H_{\perp}(\theta)}{2EI(1+\frac{1}{2}\chi_f)} \\ &= -\frac{A\chi_f\mu_0(H_x\sin\theta - H_y\cos\theta)(H_x\cos\theta + H_y\sin\theta)}{2EI(1+\frac{1}{2}\chi_f)} \end{aligned} \tag{15}$$

with $\theta(0) = \theta_0$ and $\frac{d\theta}{ds}(L) = 0$. This equation is equivalent to those found in [1,12,13], though this form looks more complicated because it makes no assumptions about the alignment of the coordinate axes and the applied field.

In the case of a nonuniform field, the integrand in Eq. (13) depends on $x(s)$ and $y(s)$, making a calculus of variations approach significantly more difficult. The Euler-Lagrange necessary conditions no longer apply.

The variation of Eq. (13) could be solved from first principles, but the dependence of $H_{\parallel}$ and $H_{\perp}$ on the integral of $\theta(s)$ makes this approach unwieldy.

Instead, a Rayleigh-Ritz method is employed to find minimum energy fiber shape(s). In this method, the fiber shape is approximated as a linear combination of basis functions plus a constant:

$$\theta(s) = \theta_0 + \sum_{i=1}^{n} \alpha_i \phi_i(s) \tag{16}$$

The basis functions are chosen so that any linear combination will automatically satisfy the boundary conditions, $\theta(0) = \theta_0$ and $\frac{d\theta}{ds}(L) = 0$. Thus, for all i, $\phi(0) = 0$ and $\dot{\phi}(L) = 0$. A family of polynomials was chosen:

$$\begin{aligned} \phi_1 &= s^2 - 2Ls \\ \phi_2 &= s^3 - 3L^2 s \\ &\vdots \\ \phi_n &= s^{n+1} - (n+1)L^n s \end{aligned} \tag{17}$$

When Eq. (16) is substituted into Eq. (13), the minimization over the infinite dimensional $\theta(s)$ turns into a finite dimensional minimization over the coefficients $\begin{bmatrix} \alpha_1 & \alpha_2 & \cdots & \alpha_n \end{bmatrix}^{\mathrm{T}}$.

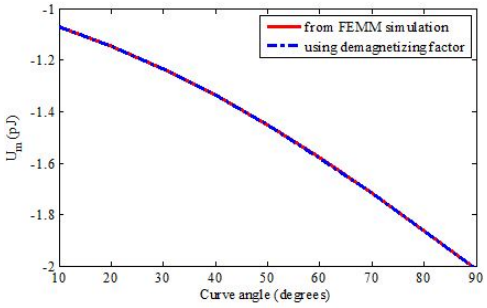

FIGURE 2. A comparison of magnetic potential energy of a curved fiber in a nonuniform field as computed using (i) finite element simulations and (ii) the demagnetizing factor approximation extended to the nonuniform field case. In this case, the two curves are essentially on top of one another, the maximum error is less than 1%, and the derivatives match up well.

This minimization problem can be solved using standard numerical techniques. While the Rayleigh-Ritz method guarantees that the boundary conditions will be satisfied, the moment balance at points along the length of the fiber will only be approximately satisfied. Increasing the number of basis functions in the approximation will improve the quality of the moment balance. In practice, three to five basis functions were found to provide sufficient accuracy to capture the behavior of the fiber.

SIMULATION

A series of simulations was performed to validate the demagnetizing factor approximation used to derive the model as well as to evaluate how well the model captures the behavior of the physical system.

Demagnetizing Factor

Finite element simulations were used to examine the demagnetizing factor approximations. The finite element simulations were performed using FEMM (Finite Element Method Magnetics), a free software package for low-frequency, two-dimensional or axisymmetric electromagnetic problems [23]. Matlab scripts were used to set up and run FEMM simulations using the OctaveFEMM toolbox.

In order to test the validity of the demagnetizing factor approximations in nonuniform fields, a study was conducted comparing the magnetic potential energy of a curved fiber in a nonuniform field (generated by a solenoid) as computed by (i) taking the difference of total field energies from two finite element simulations, one with the fiber present and one

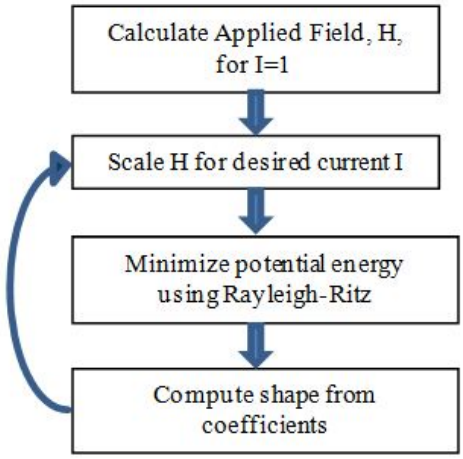

FIGURE 3. Algorithm for simulating fiber shape for different fields produced by an electromagnet. Note that the magnetic field H only needs to be calculated once. Thereafter, the field H can be simply scaled to correspond to the desired current I through the electromagnet.

without, and (ii) a demagnetizing factor approximation to the magnetic potential using a finite element model of the field without the fiber present. The results are shown in *Figure 2*. The demagnetizing factor works surprisingly well. The demagnetizing factor approximation has maximum error less than

1%, and the derivatives match up well. A more detailed study is presented in [22].

Simulated Stable Energy Configurations

A combination of Matlab scripts and FEMM simulations was used to simulate the model. An axisymmetric model of the solenoidal magnets used in the experiments was simulated in FEMM with a current of 1A. The simulated magnetic field was imported into Matlab from FEMM using the OctaveFEMM toolbox. Since the magnetic field is linear in the current, the field for different current values can be obtained by scaling the field appropriately. Thus, the magnetic field only has to be calculated once. Matlab scripts were used to find local minima of the total potential energy from Eq. (13) with respect to the n coefficients of the Rayleigh-Ritz method in Eq. (16). The Matlab fminunc command was used to automate the minimization. For the specific arrangement of magnet and fiber studied, the fiber had a single stable equilibrium point at certain current values and multiple equilibria at other values. Multiple stable equilibria correspond to multiple local minima in U . These minima were found by carefully seeding the initial guess of the coefficients for fminunc. The parameters for the system, provided in *Table I*, were chosen to match the experimental conditions of the experiment.

TABLE I. Model Parameters for simulation.

Fiber length	$L = 3.5\text{cm}$
Fiber radius	$r = 23\mu\text{m}$
Modulus	$E = 1\text{GPa}$
Moment of Inertia	$I = \pi r^4 / 4$
Magnetic suscept.	$\chi_f \approx 0.028$
Relative offset from magnet surface	$x_0 = -14.0\text{mm}$ $y_0 = -7.1\text{mm}$
Magnet length	$L_{mag} = 3.0\text{cm}$
Magnet diameter	$d_{mag} = 0.95\text{mm}$

A plot of the simulated fiber tip position for stable fiber equilibria as a function of electromagnet current will be presented along with the corresponding experimental data in the results section.

EXPERIMENTAL METHODS

Magnetic Microfibers

Magnetic materials are typically metallic or ceramic with a high elastic modulus. A wire or fiber made out of such a material would be too stiff to move a significant distance under the influence of reasonable magnetic fields. In order to make an actuator that is flexible enough to manipulate objects over millimeters range, polymer magnetic fibers are fabricated. These are hollow fibers filled with superparamagnetic nanoparticles. This combines the flexibility of a polymer with the superb magnetic properties of superparamagnetic nanoparticles to make a fiber that behaves as a flexible paramagnetic material. These fibers are significantly larger and more robust than the bead chains in the literature, e.g. [1,2]. The larger volume of magnetic material permits the fiber to develop the forces and torques required for microfluidic applications.

To fabricate the fibers, hollow cellulosic fibers (GE Healthcare) are impregnated with magnetic fluid (EFH1, FerroTec**)**. The carrier is dried, leaving a coating of superparamagnetic Fe_3O_4 nanoparticles on the fiber wall. Optionally, the particles may be fixed to the fiber wall using an additional process, such as application of Sylgard™ (Dow Corning). Fibers can be fabricated in a variety of sizes, ranging typically from 20-200 micrometers in diameter, though larger and smaller fibers are theoretically possible. Fibers are typically fabricated in lengths of 10-15cm and cut to size.

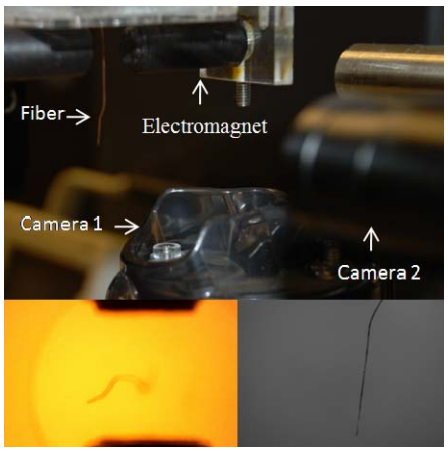

FIGURE 4. Experimental setup for magnetic microfibers. The fiber in this image is 35mm long and 46 micrometers in diameter. The fiber shown above has a small, permanent kink that can be observed in each image. (Top) A pair of electromagnets are on opposite sides of and right angles to a magnetic microfiber. The position of the magnetic microfiber is observed by two microscopes with cameras. The system is lit from above. (Bottom left) Camera 1 observes the fiber from below (Bottom right) Camera 2 views the fiber from the side.

Experimental Platform

The experimental platform for testing the performance of magnetic microfibers is shown in *Figure 4*. It consists of a magnetic microfiber hanging from an acrylic plate, with an electromagnet positioned to the side of the fiber. The Matlab XPC Target Toolbox for

real time control is used to send control signals via a Quanser Q8 Hardware-in-Loop card to a Techron amplifier, which powers the electromagnets. The Matlab Image Acquisition toolbox is used to acquire images from two microscope cameras, one positioned below the fiber and one positioned beside the fiber. Images from these cameras are processed using Matlab in order to measure the location of the fiber tip.

RESULTS AND DISCUSSION

Experimental data relating fiber tip position to electromagnet current was collected using the system with the first electromagnet (1350 turns, 0.95cm ferrite core, 3.0cm length). *Figure 5* shows the average tip position for each current value. A total of 5 independent trials were taken for each value of electromagnet current. For comparison, the experimental data is plotted against the tip position calculated from the simulated model.

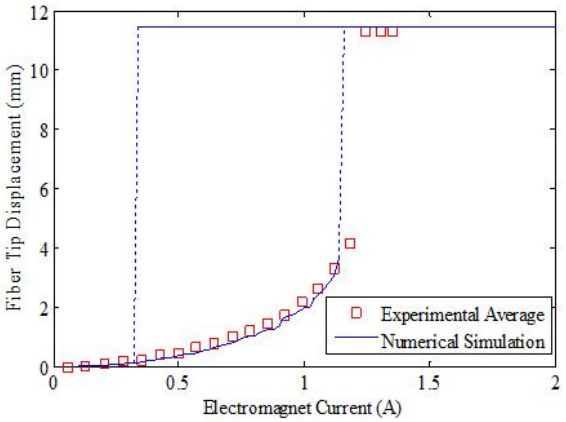

FIGURE 5. Fiber tip position vs. electromagnet current (1A corresponds to 100mT at the electromagnet's surface). Experimental points represent the average of 5 independent trials at the same current. The model and experiment both capture the position hysteresis of the fiber tip.

This position hysteresis loop is clearly visible in the image. Varying the current between 0A and 1.15A causes the fiber tip to smoothly and quickly move to the corresponding positions. At just above 1.15A, the fiber "jumps" to the electromagnet. The fiber tip displacement between 4mm and 12mm cannot be achieved using a constant current in the electromagnet. After jumping to the electromagnet, the fiber will stay attached over a wide range of currents, from 0.34A-1.15A (this was observed, but not plotted in the experimental data). When the current drops below 0.34A, the fiber tip returns to the lower curve again. This results in the position hysteresis behavior observed as current through the electromagnet is increased and decreased. This behavior is accurately predicted qualitatively and quantitatively by the simulated model. From the simulations, it is clear that the origin of the hysteresis behavior is a bifurcation in the stable equilibria of the fiber. A single stable equilibrium shape exists for high and low values of current, but a pair of stable equilibrium shapes occurs for intermediate values of current.

To further validate the model, experimental data was collected using a second electromagnet with different geometry and properties (1270 turns, 38mm diameter, 22mm length, steel core). The horizontal displacement from the base of the fiber to the center of the magnet was varied. For each displacement of the fiber base, the fiber tip position was experimentally measured as a function of magnetic field. The data and corresponding simulated model are shown in *Figure 6*. All simulated curves were generated using the same set of model parameters, except for the horizontal displacement of the fiber base. This illustrates that the model captures the behavioral trend as the fiber is repositioned in the magnetic field.

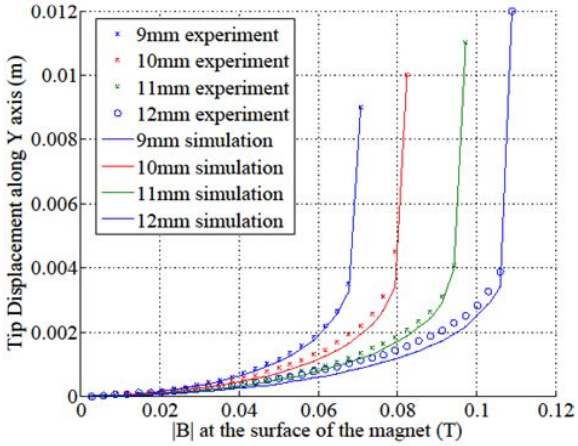

FIGURE 6. The effects of varying the offset distance y_0 between the electromagnet and the base of the fiber. The model correctly predicts the shapes of the curves and the "jump point" using a single set of parameters.

The stable shape of the fiber is very sensitive to the details of the magnetic field in its neighborhood. The magnetic field in these experiments is nonuniform, so the field depends not only on the physical properties of the electromagnet but also on the displacement between the fiber and the electromagnet. For largest displacement of the fiber base, 12mm, the experimental data and corresponding simulation display consistent, repeatable discrepancies. The simulation was performed using the experimentally measured values for the displacement of the fiber base. This is the major source of the discrepancy between the simulation and the data. The discrepancy could be essentially eliminated by allowing the

simulation to find the best fit, as opposed to experimentally measured, displacement of the fiber base.

In these experiments, the magnetic field is nearly orthogonal to the rest position of the fiber. If the magnetic field were uniform and orthogonal to the rest position of the fiber, then the rest position would be a stable shape regardless of the intensity of the field. Deflection of the fiber at low field strengths occurs only in the presence of a nonuniform field. Deflection at low fields is predicted by the present model, but is not predicted by previous models that consider only uniform fields [1,3,15,24].

RIGID BAR MODEL

In order to understand the origins of the bifurcations that lead to position hysteresis, it is illustrative to examine a simpler model of the system. Consider the fiber as a rigid bar attached to a torsional spring at the base, as seen in *Figure 7*.

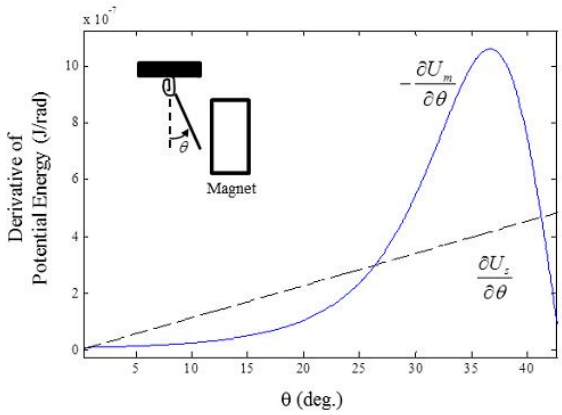

FIGURE 7. The rigid bar model for the fiber graphically illustrates the bifurcation in stable equilibrium shapes of the fiber.

Then the strain energy is simply $U_s = \frac{1}{2} k_s \theta^2$, where k_s is the torsional spring constant and θ is the deflection of the spring. In this case, the "shape" of the fiber is entirely described by the scalar variable θ. The magnetic potential energy U_m is as defined in Eq. (12), though θ no longer depends on s. In the following discussion, U_m is based on a magnetic dipole, rather than a finite element model of the physical magnet.

The minimization of energy $U = U_s + U_m$ is now with respect to the scalar variable θ and may be solved using standard techniques from calculus. A value of θ for which

$$\frac{dU_s}{d\theta} = -\frac{dU_m}{d\theta} \tag{18}$$

is a critical point of the energy. A critical point corresponds to a local minimum, local maximum, or saddle point of U. It will be a local minimum, i.e. a stable shape of the fiber, if

$$\frac{d^2U_s}{d\theta^2} + \frac{d^2U_m}{d\theta^2} > 0 \tag{19}$$

This has a convenient graphical interpretation, illustrated in *Figure 7*. The curves for $\frac{dU_s}{d\theta}$ and $-\frac{dU_m}{d\theta}$ are plotted as a function of θ. These curves can be interpreted as torques acting on the fiber. Points where the two curves intersect are critical points, i.e. equilibrium shapes of the fiber. In *Figure 7*, there are three critical points, at 0.8°, 26.3°, and 41.2°. Applying the criterion from Eq. (19) shows that the critical points at 0.8° and 41.2° correspond to a stable shape of

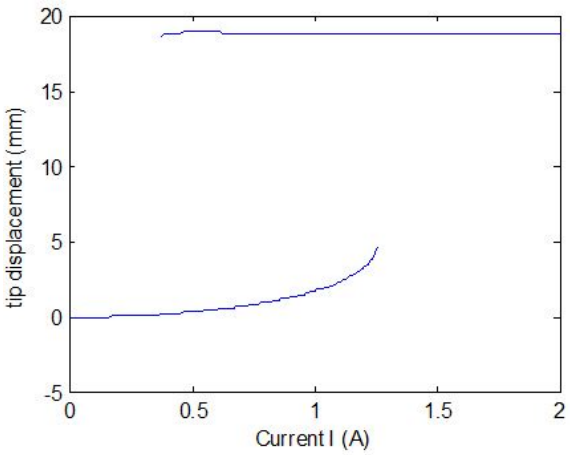

FIGURE 8. Stable tip positions as a function of current through the electromagnet for the rigid bar model.

the fiber, since the slope of $\frac{dU_s}{d\theta}$ is large than the slope of $-\frac{dU_m}{d\theta}$. Similarly, the critical point at 26.3° corresponds to an unstable shape of the fiber. The curve $-\frac{dU_m}{d\theta}$ plotted in *Figure 7* corresponds to an intermediate magnetic field, which provides two stable equilibria, one close to the rest shape (small θ) and one close to the magnet (large θ). Varying current through the magnet simply scales U_m and hence scales the curve $-\frac{dU_m}{d\theta}$ in proportion to current. The appearance and disappearance of critical points can be directly inferred from the plot by imagining what happens as the $-\frac{dU_m}{d\theta}$ curve is scaled. For small

currents, the peak of the $-\frac{dU_m}{d\theta}$ curve falls below the line for $\frac{dU_s}{d\theta}$. In this case the rightmost two critical points disappear, leaving a single stable equilibrium point corresponding to a small deflection of the fiber. For large current, the trough of $-\frac{dU_m}{d\theta}$ rises above the line for $\frac{dU_s}{d\theta}$. In this case the leftmost two critical points disappear, leaving a single stable equilibrium point corresponding to a large deflection of the fiber. This appearance and disappearance of stable equilibria leads to the observed position hysteresis. *Figure 8* plots the tip deflection of the rigid bar model as a function of the electromagnet current.

The rigid bar model captures the qualitative behavior of the fiber and helps illuminate the source of the hysteresis. By fitting the model parameters in the rigid bar model, it is even possible to fit the experimental data reasonably well, but it is more difficult to relate these model parameters back to the underlying physical parameters in the experiment. The rigid bar model is most useful for gaining insight into the source of the hysteresis behavior.

CONCLUSION

A detailed derivation of the model for fiber shape in a nonuniform field was presented. Simulation of the model matches the experimental data both qualitatively and quantitatively. The model accurately captures the hysteresis behavior of the fiber.

The model only requires the magnetic field to be computed once in order to compute the stable configurations for varying current through the electromagnet. This makes the model computationally faster than solving the fully coupled electromagnetic and solid mechanics problem using finite element techniques. This computational speed makes the model useful for design actuators based on magnetic microfibers, since many configurations can be simulated and studied in a reasonable amount of time. This computational speed also makes it feasible to solve the inverse problem. That is, electromagnet currents and fiber shape could be observes, and then the magnetic and mechanical properties of the fiber could be deduced from these measurements.

A rigid bar model was introduced to illustrate the source of the hysteresis behavior. In this model, the appearance and disappearance of stable shapes of the fiber may be observed graphically. The rigid bar model is more useful qualitatively than quantitatively.

A large number of new devices and applications based on magnetic microfibers have recently been developed, from flagella and cilia for swimming robots to fluid manipulation to an artificial butterfly proboscis. The model presented in this paper will serve as an important tool for characterizing the properties of and designing devices based on magnetic microfibers. As future work, the model will be extended to consider dynamics, which will enable model-based feedback control of magnetic microfiber devices.

ACKNOWLEDGMENT

The authors would like to thank Carmel Majidi for helpful discussions and to thank Sriram Ravindren, John Kelley, and Justin Mattimore for preliminary work with the experimental platform. This work was funded in part by NSF EFRI Grant #0937985 and by Southeastern Center for Electrical Engineering Education Grant #SCEEE-08-0002.

REFERENCES

[1] Goubault, C., et al., "Flexible magnetic filaments as micromechanical sensors", *Phys Rev Lett*, Vol. 91, No. 26, 2003, pp. 260802.

[2] Biswal, S. L., Gast, A. P., "Mechanics of semiflexible chains formed by poly(ethylene glycol)-linked paramagnetic particles", *Phys Rev E*, Vol. 68, No. 2, 2003, pp. 021402.

[3] Cebers, A., "Flexible magnetic filaments", *Curr Opin Colloid In*, Vol. 10, No. 3-4, 2005, pp. 167-175.

[4] Tsai, C., et al., "Nanoporous artificial proboscis for probing minute amount of liquids", *Nanoscale*, Vol. 3, No. 11, 2011, pp. 4685-4695.

[5] Zhang, H., Widom, M., "Field-induced forces in colloidal particle chains", *Phys Rev E*, Vol. 51, No. 3, 1995, pp. 2099-103.

[6] Furst, E. M., et al., "Permanently linked monodisperse paramagnetic chains", *Langmuir*, Vol. 14, No. 26, 1998, pp. 7334-7336.

[7] Dreyfus, R., et al., "Microscopic artificial swimmers", *Nature*, Vol. 437, No. 7060, 2005, pp. 862-865.

[8] Gauger, E., Stark, H., "Numerical study of a microscopic artificial swimmer", *Phys Rev E*, Vol. 74, No. 2, 2006, pp. 021907.

[9] Bell, D.J., et al., "Flagella-like propulsion for microrobots using a nanocoil and a rotating electromagnetic field", in Proc of ICRA., 2007, pp. 1128-1133.
[10] Aharoni, A., "Traction force on paramagnetic particles in magnetic separators", *IEEE T Magn*, Vol. MAG-12, No. 3, 1976, pp. 234-5.
[11] Cebers, A., "Dynamics of an elongated magnetic droplet in a rotating field", *Phys Rev E*, Vol. 66, No. 6, 2002, pp. 061402-1.
[12] Morozov, K. I., Engel, A., Lebedev, A.V., "Shape transformations in rotating ferrofluid drops", *Europhys Lett*, Vol. 58, No. 2, 2002, pp. 229-35.
[13] Cebers, A., "Dynamics of elongated magnetic droplets and elastic rods in magnetic field", *J Magn Magn Mater*, Vol. 289, 2005, pp. 335-8.
[14] Moon, F.C., Yih-Hsing Pao, "Magnetoelastic buckling of a thin plate", *J Appl Mech*, Vol. 35, No. 1, 1968, pp. 53-8.
[15] Moon, F.C., Pao, Y. H., "Vibration and Dynamic Instability of Beam-Plate in Transverse Magnetic Field", *J Appl Mech*, Vol. 36, No. 1, 1969, pp. 92.
[16] Moon, F.C., "Problems in magneto-solid mechanics", *Mechanics Today*, Vol. 4, 1978, pp. 307-390.
[17] Moon, F.C., Holmes, P.J., "Magnetoelastic Strange Attractor", *J Sound Vibrat*, Vol. 65, No. 2, 1979, pp. 275-296.
[18] J.M. Gere, S. Timoshenko, *Mechanics of Materials*, 4th ed., PWS Pub Co., Boston, 1997.
[19] J.D. Jackson, *Classical Electrodynamics*, 3rd ed., Wiley, New York, 1999.
[20] A. Aharoni, *Introduction to the Theory of Ferromagnetism*, 2nd ed., Oxford University Press, Oxford; New York, 2000.
[21] J.A. Stratton, *Electromagnetic Theory*, Wiley, Hoboken, NJ, 2007.
[22] Karve, H.D., "Modeling and Characterization of Magnetic Microfibers", MS thesis, Clemson University, 2012.
[23] Meeker, D. "Finite Element Method Magnetics", Last Updated 06/26/2011, Accessed 10/15/2011, http://www.femm.info/wiki/HomePage .
[24] Cebers, A., "Dynamics of a chain of magnetic particles connected with elastic linkers", *J Phys-Condens Mat*, Vol. 15, No. 15, 2003, pp. 1335-1344.

AUTHORS' ADDRESSES
Richard E. Groff, Ph.D.
Harshwardhan Karve
Meng Li
Dept. of Electrical and Computer Engineering
Clemson University
Clemson, SC 29634
UNITED STATES

Alexander Tokarev
Kostantin G. Kornev
Dept. of Materials Science and Engineering
Clemson University
Clemson, SC 29634
UNITED STATES